expected. For L = 12.7mm, the resonance occurs at f_r = 4.74GHz with a bandwidth ($|S_{11}| < -10$dB) of 9.2%. It is found that the resonant frequency is lower than that of the previous perpendicular-feed configuration (f_r = 5.33GHz) [6]. As compared with the previous version, the present configuration offers one more degree of

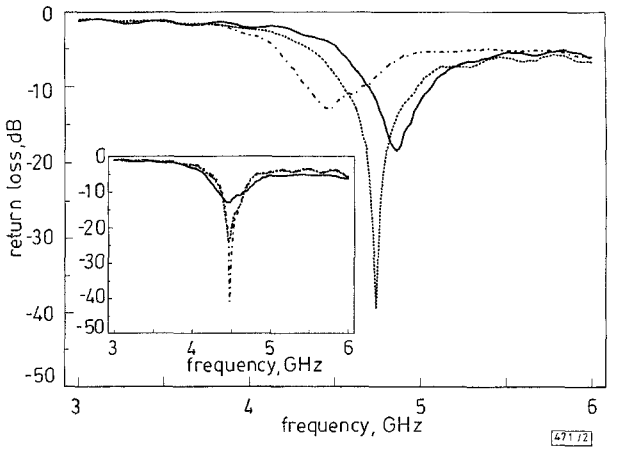

Fig. 2 *Measured return losses for different slot lengths*

Inset : Measured return losses for different stub lengths
——— L = 11.5mm (inset: L_s = 3.2mm)
····· L = 12.7mm (inset: L_s = 5.1mm)
–·–·– L = 13.5mm (inset: L_s = 5.7mm)

freedom for impedance matching by providing a tuning stub. The inset of Fig. 2 shows the return losses for three different stub lengths L_s = 3.2, 5.1, 5.7mm with L = 13.5mm. With reference to the inset Figure, the impedance matching is improved continuously as the stub length is increased from 3.2 to 5.7mm. By changing the stub length an excellent match can also be obtained for L = 11.5mm. The results are summarised in Table 1. With reference

Table 1: Summary of impedance matching for different slot and stub lengths

Slot L	Stub L_s	f_r	BW	min. $\|S_{11}\|$
mm	mm	GHz	%	dB
11.5	14.2	4.6	10.0	–47.4
12.7	3.2	4.74	8.4	–39.3
13.5	5.7	4.48	5.3	–40.8

to the Table, the bandwidth is increased with decreasing slot length, as discussed in [6]. The effects of the offsets x_d and y_d on the return loss were also studied. It was found that the offsets are two other degrees of freedom for changing the input impedance. The results are very similar to those in [6] and are omitted here to conserve space.

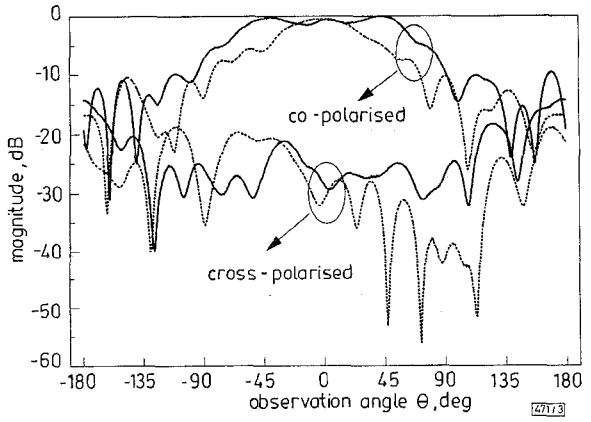

Fig. 3 *Measured radiation field patterns*

——— *E*-plane
····· *H*-plane

Fig. 3 shows the measured *E*- and *H*-plane radiation patterns for L = 13.5mm, L_s = 5.7mm and f = 4.48GHz. With reference to the Figure, the broadside patterns are obtained which are very similar to those of the previous configuration [6]. As is desirable, the front-to-back ratios are very high, ~18 and 16dB for the *E*- and *H*- plane patterns, respectively. Conversely, the crosspolarised fields are very weak, ~30dB less than the copolarised fields in the broadside direction (θ = 0).

The antenna gain of the present configuration for L = 13.5mm and L_s = 5.7mm was also measured. Again, the result was similar to that of the previous configuration and is omitted in this Letter for brevity.

Conclusion: We have investigated the slot-coupled cylindrical DRA with a proximity feed on a perpendicular substrate. The characteristics of the new configuration are very similar to those of the previous configuration [6]. As compared with the previous configuration, this present version has two advantages. First there is no need for direct connection between the feedline and the coupling slot and secondly it provides a tuning stub. The choices of the feedline distance d_f and the removed ground plane size $p \times q$ are in an *ad hoc* manner and should not be critical in practical designs.

Acknowledgments: The work is supported by the UGC Earmarked Research Grant.

14 July 1997
Electronics Letters Online No: 19971161

K.W. Leung and M.W. To (*Department of Electronic Engineering, City University of Hong Kong, Kowloon, Hong Kong*)

References

1 LONG, S.A., MCALLISTER, M.W., and SHEN, L.C.: 'The resonant cylindrical dielectric cavity antenna', *IEEE Trans.*, 1983, **AP-31**, pp. 406–412
2 KRANENBURG, R.A., and LONG, S.A.: 'Microstrip transmission line excitation of dielectric resonator antennas', *Electron. Lett.*, 1988, **24**, pp. 1156–1157
3 KRANENBURG, R.A., LONG, S.A., and WILLIAMS, J.T.: 'Coplanar waveguide excitation of dielectric resonator antennas', *IEEE Trans.*, 1991, **AP-39**, pp. 119–122
4 MARTIN, J.T.H.ST., ANTAR, Y.M.M., KISHK, A.A., and ITTIPIBOON, A.: 'Dielectric resonator antenna using aperture coupling', *Electron. Lett.*, 1990, **26**, pp. 2015–2016
5 LEUNG, K.W., CHOW, K.Y., LUK, K.M., and YUNG, E.K.N.: 'Excitation of dielectric resonator antenna using a soldered-through probe', *Electron. Lett.*, 1997, **33**, pp. 349–350
6 LEUNG, K.W., and TO, M.W.: 'Aperture-coupled dielectric resonator antenna with a perpendicular feed', *Electron. Lett.*, 1997, **33**, pp. 1000–1001
7 BUCK, A.C., and POZAR, D.M.: 'Aperture-coupled microstrip antenna with a perpendicular feed', *Electron. Lett.*, 1986, **22**, pp. 125–126
8 POZAR, D.M., and JACKSON, R.W.: 'An aperture-coupled microstrip antenna with a proximity feed on a perpendicular substrate', *IEEE Trans.*, 1987, **AP-35**, pp. 728–731

Noise-assisted signal transmission via stochastic resonance in a diode nonlinearity

X. Godivier, J. Rojas-Varela and F. Chapeau-Blondeau

Indexing terms: Nonlinear systems, Circuit theory

The nonlinear effect of noise-assisted signal transmission via stochastic resonance is demonstrated in a diode circuit. This study establishes one of the simplest conceivable settings for stochastic resonance, accompanied by a complete theoretical description, and it may serve as a useful model for further investigation of the effect.

Stochastic resonance is a nonlinear effect consisting of an enhancement of the transmission of a signal by certain nonlinear systems resulting from noise addition to the system. This paradoxical effect was introduced some fifteen years ago in the context of climate

dynamics [1]. It has gradually been reported in a variety of systems, including lasers, neurons, superconducting devices, electronic circuits [1], and its connections with other useful noise techniques have been discussed [2]. Among electronic circuits shown to exhibit stochastic resonance are a Schmitt trigger with both a threshold and hysteretic nonlinearity [3], and a chaotic Chua's circuit [4]. These nonlinear circuits are complicated enough to hinder an exact theoretical treatment of the effect, which was essentially exhibited through experiments or numerical simulations. Only recently has a theory been proposed that models stochastic resonance in a general class of nonlinear systems [5]. Based on both this theory and an experimental realisation, we prove here that a nonlinear system as simple as a diode nonlinearity contains the essential ingredients necessary for exhibiting a form of stochastic resonance, and, as a result, stands as a model for one of the simplest conceivable stochastic resonators.

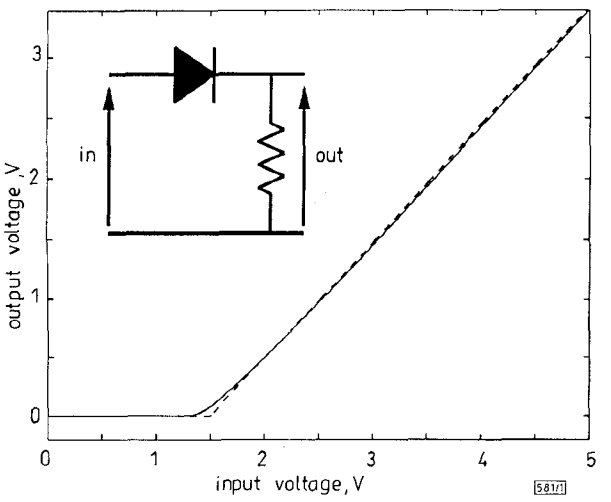

Fig. 1 *Diode circuit and its input-output static characteristics*

——— experimental results
- - - - simple theoretical model

Consider the circuit of Fig. 1, where the input voltage consists of the sum $s(t) + \eta(t)$, with $s(t)$ a T_s-periodic signal and $\eta(t)$ a stationary white noise with the probability density function $f_\eta(u)$. The output voltage $y(t)$ results as a nonstationary (cyclostationary) random signal, bearing a correlation to the periodic input $s(t)$. As we shall show, conditions exist in which this correlation can be reinforced when the input noise level is raised.

This correlation is quantified here by means of the output autocorrelation function

$$R_{yy}(k\Delta t) = \frac{1}{N}\sum_{j=0}^{N-1} E[y(j\Delta t)y(j\Delta t + k\Delta t)] \quad (1)$$

where, to compare theory and experiment, we use a discrete-time formulation in which the signals are sampled at a step $\Delta t \ll T_s = N\Delta t$.

The output power spectral density follows, from a discrete Fourier transform of R_{yy} over an integer number $2M$ of period T_s, as

$$P_{yy}(\ell\Delta\nu) = \sum_{k=-MN}^{MN-1} R_{yy}(k\Delta t)\exp\left(-i2\pi\frac{k\ell}{2MN}\right) \quad (2)$$

with the frequency resolution $\Delta\nu = 1/(2MN\Delta t)$.

The noise input $\eta(t)$ is responsible for a broadband continuous background in P_{yy} out of which spectral lines emerge at integer multiples of $1/T_s$ as a consequence of the influence of the periodic input $s(t)$. The emergence of these lines out of the noise background can be made more pronounced by an increase in the input noise level, the signature of stochastic resonance. This effect can be quantified by a signal-to-noise ratio (SNR) at the output, defined as the power contained in the spectral line alone at frequency n/T_s divided by the power contained in the noise background in a small frequency band ΔB around n/T_s.

The theory of [5] predicts that the output power spectral density is

$$P_{yy}(\ell\Delta\nu) = \overline{\mathrm{var}(y)} + \sum_{n=-\infty}^{+\infty} |\bar{Y}_n|^2\hat{\delta}(\ell - 2Mn) \quad (3)$$

with $\hat{\delta}(0) = 2MN$ and $\hat{\delta}(j) = 0$ for an integer $j \neq 0$, leading to an output SNR at frequency n/T_s:

$$\mathbf{R}\left(\frac{n}{T_s}\right) = \frac{|\bar{Y}_n|^2}{\overline{\mathrm{var}(y)}\Delta t\Delta B} \quad (4)$$

In eqns. 3 and 4:

$$\bar{Y}_n = \frac{1}{N}\sum_{j=0}^{N-1} E[y(j\Delta t)]\exp\left(-i2\pi\frac{jn}{N}\right) \quad (5)$$

is the order n Fourier coefficient of the T_s-periodic output expectation $E[y(j\Delta t)]$ computable as

$$E[y(t)] = \int_{-\infty}^{+\infty} g(u)f_\eta[u - s(t)]du \quad (6)$$

Also, in eqns. 3 and 4:

$$\overline{\mathrm{var}(y)} = \frac{1}{N}\sum_{j=0}^{N-1} \mathrm{var}[y(j\Delta t)] \quad (7)$$

with the T_s-periodic output variance $\mathrm{var}[y(t)] = E[y^2(t)] - E^2[y(t)]$ computable with

$$E[y^2(t)] = \int_{-\infty}^{+\infty} g^2(u)f_\eta[u - s(t)]du \quad (8)$$

In eqns. 6 and 8, the function $g(u)$ represents the input-output static characteristics of the nonlinear circuit realising $y = g(s + \eta)$. Fig. 1 displays the experimental characteristics that have been measured for the circuit shown. We chose the diode (a red LED TLHR 5400 from TEMIC) so as to have almost linear characteristics above the conduction threshold, being well approximated by the simple model $g(u) = u - V_{th}$ for $u > V_{th}$, and $g(u) = 0$ otherwise, with $V_{th} = 1.5$V.

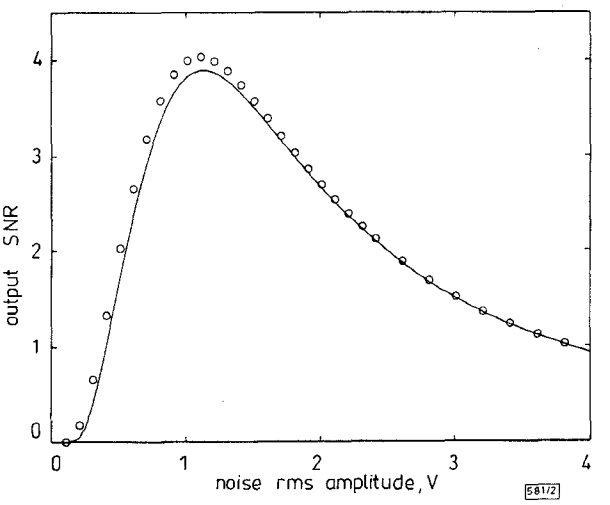

Fig. 2 *Experimental and theoretical output SNR at fundamental $1/T_s$ against σ*

Sinusoidal input signal $s(t) = A\cos(2\pi t/T_s)$ with $A = 1$V and zero-mean Gaussian noise $\eta(t)$ with rms amplitude σ
O Experimental
——— Theoretical

In the case where $\eta(t)$ is a zero-mean Gaussian noise with rms amplitude σ, eqn. 6 then leads to

$$E[y(t)] = \frac{\sigma}{\sqrt{2}}\left\{\frac{1}{\sqrt{\pi}}\exp[-z^2(t)] - z(t)\mathrm{erfc}[z(t)]\right\} \quad (9)$$

and eqn. 8 to

$$E[y^2(t)] = \frac{\sigma^2}{2}\left\{[1+2z^2(t)]\mathrm{erfc}[z(t)] - \frac{2}{\sqrt{\pi}}z(t)\exp[-z^2(t)]\right\} \quad (10)$$

with $z(t) = [V_{th} - s(t)]/(\sigma\sqrt{2})$.

From eqns. 9 and 10, the output SNR of eqn. 4 has been computed; also, this quantity has been experimentally evaluated on the circuit of Fig. 1. Both results are shown in Fig. 2 (when $\Delta B = 1/T_s$), which reveals very close agreement between theory and experiment, taking into account the simple linear model adopted

for the static characteristics. The nonmonotonic evolution of the output SNR with the input noise level, which peaks at a maximum value for an optimal non-zero noise level, demonstrates the stochastic resonance effect.

The stochastic resonance here relies on a simple threshold system, with a subliminal signal whose transmission is only possible in the presence of the noise, with the maximum efficacy for an optimum noise level being explicitly predictable by theory, for instance as a function of the noise distribution. Other situations exist where a subliminal signal or a threshold are not necessary for stochastic resonance [5, 6], or where the signal can be either a high-frequency carrier modulated by a low-frequency message, or a broadband aperiodic signal [7 – 9].

28 August 1997
Electronics Letters Online No: 19971148

X. Godivier and F. Chapeau-Blondeau (*Laboratoire d'Ingénierie des Systèmes Automatisés (LISA), Faculté des Sciences, Université d'Angers, boulevard Lavoisier, 49000 Angers, France*)

J. Rojas-Varela (*Institut Universitaire de Technologie, Université d'Angers, boulevard Lavoisier, 49000 Angers, France*)

References

1 WIESENFELD, K., and MOSS, F.: 'Stochastic resonance and the benefits of noise: From ice ages to crayfish and SQUIDs', *Nature*, 1995, **373**, pp. 33–36
2 GAMMAITONI, L.: 'Stochastic resonance and the dithering effect in threshold physical systems', *Phys. Rev. E*, 1995, **52**, pp. 4691–4698
3 FAUVE, S., and HESLOT, F.: 'Stochastic resonance in a bistable system', *Phys. Lett. A*, 1983, **97**, pp. 5–7
4 ANISHCHENKO, V.S., SAFONOVA, M.A., and CHUA, L.O.: 'Stochastic resonance in Chua's circuit', *Int. J. Bifurcation Chaos Appl. Sci. Eng.*, 1992, **2**, pp. 397–401
5 CHAPEAU-BLONDEAU, F., and GODIVIER, X.: 'Theory of stochastic resonance in signal transmission by static nonlinear systems', *Phys. Rev. E*, 1997, **55**, pp. 1478–1495
6 BEZRUKOV, S.M., and VODYANOY, I.: 'Stochastic resonance in non-dynamical systems without response thresholds', *Nature*, 1997, **385**, pp. 319–321
7 ANISHCHENKO, V.S., SAFONOVA, M.A., and CHUA, L.O.: 'Stochastic resonance in Chua's circuit driven by amplitude or frequency modulated signals', *Int. J. Bifurcation Chaos Appl. Sci. Eng.*, 1994, **4**, pp. 441-446
8 COLLINS, J.J., CHOW, C.C., CAPELA, A.C., and IMHOFF, T.T.: 'Aperiodic stochastic resonance', *Phys. Rev. E*, 1996, **54**, pp. 5575–5584
9 CHAPEAU-BLONDEAU, F.: 'Noise-enhanced capacity via stochastic resonance in an asymmetric binary channel', *Phys. Rev. E*, 1997, **55**, pp. 2016–2019

Algorithm for mapping between information bits and channel symbols in MTCM codes

I.S. Jin, K.C. Whang, K. Cho, J.Y. Ahn and H.S. Oh

Indexing term: Trellis coded modulation

An algorithm for mapping between information bits and channel symbols in multiple trellis-coded modulation (MTCM) codes with M-PSK signal sets is proposed. The core of the algorithm assigns information bits with a Hamming distance in proportion to the sum of the Euclidean distance to each M-PSK symbol. The analytical results show that the additional gains from applying the algorithm can be achieved with little or no loss.

Introduction: Trellis-coded modulation (TCM) has received much attention for bandwidth and power efficient transmission of data. Ungerboeck [1] improved the error-event probability (EEP) by using a signal mapping technique called 'set partitioning', while most earlier works on TCM concentrated on minimising the EEP. For bitwise communication systems, such as image data transmission systems, decreasing the post-decoding information bit error rate (IBER) is more important than only minimising the EEP. Du and Kasahara succeeded in improving the IBER by using Gray code mapping [2]. In [3], Umeda *et al.* expanded this idea by using minimum Hamming distance (MHD) mapping.

However, MHD mapping cannot be applied to multiple trellis-coded modulation (MTCM) schemes directly because more than one channel symbol is assigned to each trellis branch in MTCM. We found that the performance is even worse than that of conventional MTCM schemes if the MHD mapping is directly applied to MTCM schemes. Therefore, we need another algorithm to apply the MHD mapping concept in MTCM schemes. In this Letter, we outline a simple algorithm for mapping between information bits and channel symbols in MTCM schemes and to improve the performance of MTCM schemes by reducing the BER with little or no loss.

Basic rules: Proper bit-to-symbol mapping can reduce the number of erroneous bits. When the BER is the performance measure, the bit assignment for k^* M-PSK symbols in an MTCM scheme is important. The parameter k^* is referred to as the multiplicity of the code and represents the number of M-PSK symbols allocated to each branch in the trellis diagram. Information bits are mapped on groups of k^* M-PSK symbols. The core of the algorithm assigns information bits with a Hamming distance in proportion to the sum of the Euclidean distance to each k^* M-PSK symbol. Following these rules, we have constructed a simple algorithm for mapping between information bits and channel symbols. We have not attempted to modify the channel signal set obtained by Divsalar [4] or Periyalwar [5] because it is beyond the scope of this Letter.

Algorithm: Let us define the number of states s, the number of parallel transitions N_p and the number of input bits b. The procedure is divided into two parts. The first part is for the case that N_p is < 4, the second is for the case that N_p is ≥ 4. The steps for the bit assignment for k^* M-PSK symbols in an MTCM scheme are as follows:

(i) If N_p is < 4, then sort a pair of binary input bits in order of their large binary Hamming distance. For example, if $b = 3$, then we have, for example, {000, 111}, {001, 010}, {011, 101} and {100, 110}.
(ii) Assign, sequentially, a pair of input bits with a large binary Hamming distance to k^* M-PSK symbols with a large sum of Euclidean distances in the branch emanating from the same state.
(iii) Repeat steps (i)-(ii) for the other branch in the other state.
(iv) Stop.

If N_p is ≥ 4, the procedure is divided into two parts again. One is the lower $\log_2 N_p$ bits assignments of b bits, the other is the higher b–$\log_2 N_p$ bits assignments of b bits.
(v) Carry out steps (vi)-(viii) for the lower $\log_2 N_p$ bits assignments of b bits.
(vi) Transform the decimal number from 0 to N_p into a binary number, and then sort a pair of binary bits in order of their large binary Hamming distance.
(vii) Select a pair of parallel transitions within each inter-signal sets and compute the sum of the Euclidean distance.
(viii) Assign $\log_2 N_p$ information bits with a large Hamming distance in proportion to the large sum of Euclidean distance to each k^* M-PSK symbols. Go to step (xiv).
(ix) Carry out steps (x)-(xiii) for the higher b–$\log_2 N_p$ bit assignments of b bits.
(x) Transform the decimal number from 0 to $2^{\log_2 N_p}$ into a binary number, and then sort a pair of binary bits in order of their large binary Hamming distance.
(xi) Select the first branch in each parallel transition and then compute the sum of the Euclidean distance between a pair of transitions, selected one by one from each group.
(xii) Assign b–$\log_2 N_p$ information bits with a Hamming distance in proportion to the sum of Euclidean distance to each k^* M-PSK symbol.
(xiii) Repeat steps (xi)-(xii) for all possible combinations.
(xiv) Stop.

Below, we show, as an example, the difference between natural mapping and the proposed mapping for the 4-state rate 4/6 ($k^* = 2$) 8-PSK MTCM signal set obtained by Divsalar [4]. The trellis diagram for the example is given in [4].

Natural mapping: (information bits/8-PSK symbols)

Proposed mapping: